Enhanced Output Performance of All-Solution-Processed Organic Thermoelectrics: Spray Printing and Interface Engineering

Seongkwon Hwang,[⊥] Inho Jeong,[⊥] Juhyung Park, Jae-Keun Kim, Heesuk Kim, Takhee Lee, Jeonghun Kwak,* and Seungjun Chung*

Cite This: *ACS Appl. Mater. Interfaces* 2020, 12, 26250−26257

Read Online

ACCESS | 📊 Metrics & More | 📄 Article Recommendations | SI Supporting Information

ABSTRACT: We report two organocompatible strategies to enhance the output performance of all-solution-processed poly(3,4-ethylenedioxythiophene):poly-(styrenesulfonate) (PEDOT:PSS) thermoelectric generators (TEGs): introducing an additive spray printing process and functionalized polymer interlayers to reduce the module resistance. The spray printing enabled the deposition of 1-μm-thick PEDOT:PSS layers with a high degree of design freedom, resulting in a significantly reduced sheet resistance of 16 Ω sq^{-1} that is closely related to the thermoelectric output performance. Also, by inserting an ultrathin silane-terminated polystyrene (PS) interlayer between the PEDOT:PSS thermoelectric layers and inkjet-printed Ag interconnects selectively, the contact resistivity extracted by the transmission line method was reduced from 6.02×10^{-2} to 2.77×10^{-2} Ω cm^2. We found that the PS interlayers behaved as a thin tunneling layer, which facilitated the carrier injection from the inkjet-printed Ag electrodes into the PEDOT:PSS films by field emission with an effectively lowered energy barrier. The activation energy was also extracted using the Richardson equation, resulting in a reduction of 2.59 ± 0.04 meV after the PS treatment. Scalable plastic-compatible processability and selective interface engineering enabled to demonstrate the flexible 74-leg PEDOT:PSS TEGs exhibiting the open-circuit voltage of 9.21 mV and the output power of 2.23 nW at a temperature difference of 10 K.

KEYWORDS: *organic thermoelectrics, flexible, inkjet printing, contact resistance, PEDOT:PSS, interface engineering*
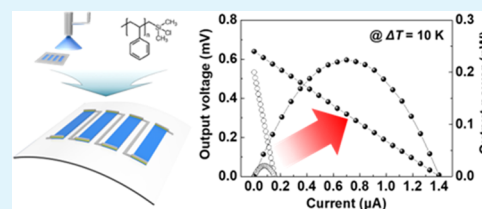
1. INTRODUCTION

Thermoelectric generators (TEGs) have gained a substantial amount of attention as sustainable and renewable energy harvesters that can directly convert waste heat into usable electricity.[1−9] In recent decades, although Bi$_2$Te$_3$-based or nanocrystal inorganic thermoelectric (TE) materials have been intensively developed from the perspective of TE output characteristics, interest in solution-processable organic TE materials has also tremendously increased owing to their low cost, low temperature, and nonvacuum processability.[4−8,10−14] Moreover, their inherent flexibility enables the production of geometrically versatile energy harvesting systems with a high degree of design freedom.[15] Among organic TE material candidates, poly(3,4-ethylenedioxythiophene):poly-(styrenesulfonate) (PEDOT:PSS) has been widely investigated due to its advantages, including a relatively low thermal conductivity and flexibility and light weight compared to its conventional inorganic counterparts.[16−20] In addition, PE-DOT:PSS-based TEGs can be facilely implemented using additive printing technologies that offer great opportunities for the realization of low-cost energy harvesting systems on large-area flexible platforms.[20−24] Despite these advantages, their low output performance is a critical drawback for their use in practical applications; therefore, there has been a lot of effort to enhance their TE characteristics by introducing chemical de-doping processes, post-treatments with a super-acid

solution, and hybrid composites with high-performance inorganic TE materials.[21,23,25−31]

In addition to achieving a high figure of merit ($zT = S^2\sigma T/\kappa$, where S is the Seebeck coefficient, σ is the electrical conductivity, κ is the thermal conductivity, and T is the absolute temperature) that is fully dependent on the characteristics of the TE materials, an optimized module design with a minimized parasitic power loss can be a key pathway to improving TE output characteristics.[8,9,13,18,32,33] The maximum output power can be expressed as follows

$$P_{max} = N(S\Delta T)^2 / 4(R_i + 2R_b) \qquad (1)$$

where N is the number of TE elements, ΔT is the absolute temperature difference, R_i is the internal resistance, and R_b is the boundary electrical resistance for a single TE leg.[34] Thus, a reduction in the internal resistance (*i.e.*, TE leg resistance) as well as an increase in the number of TE legs are the most practical routes to enhance the output power in a given set of
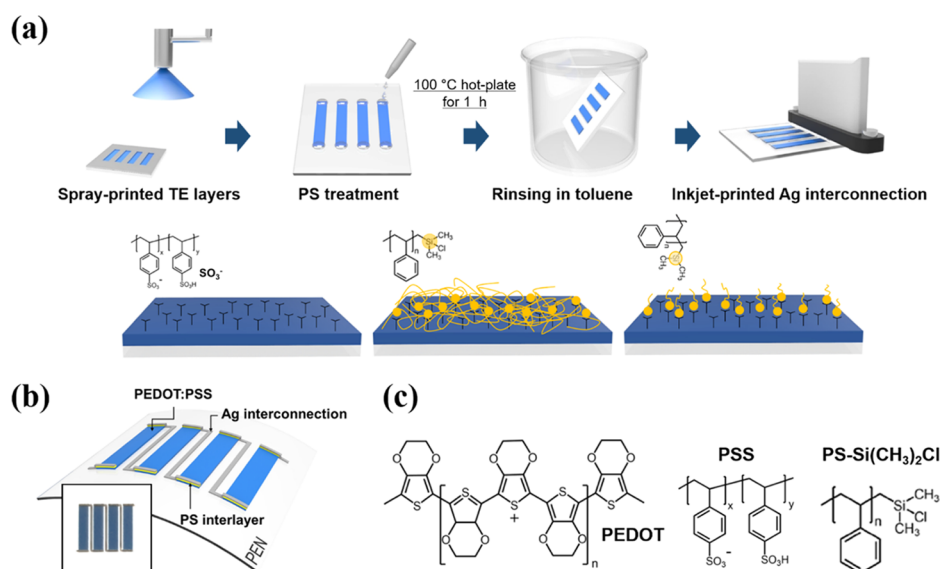
Figure 1. (a) Schematic of the fabrication process and binding scheme of PS-Si(CH$_3$)$_2$Cl onto PEDOT:PSS TE layers. (b) Scheme of all-solution-processed PEDOT:PSS thermoelectrics (magnified optical image of a 4-leg TEG is also included in the inset). (c) Chemical structures of PEDOT:PSS and functionalized PS.

conditions. However, the thermal conductivity of TE elements is also proportionally increased by enhancing their electrical conductivity, which can typically result in a less secured temperature difference.[35] Therefore, a reduction in the boundary electrical resistance across the contact area, which is expressed as $R_b = R_c/A$, where R_c and A are the contact resistivity and the contact area, respectively, is also necessary without increasing the thermal conductivity of TE layers. Specifically, a high contact resistance is typically exhibited between organic TE elements and metal electrodes due to a huge energy barrier accounting for a large portion of the total module resistance.[36] Many studies have been conducted to reduce the contact resistance, for example the introduction of additional solvents during the active layer formation, ion implantation onto TE materials, and the introduction of molecular or polymer interlayers between organic−inorganic interfaces.[37−40] However, because most of the previously reported approaches require time-consuming and complicated processing steps or additional patterned masks, further straightforward strategies that are compatible with low-cost additive manufacturing onto flexible platforms are highly desirable.

In this context, we propose organocompatible facile methodologies to improve the output characteristics of all-solution-processed flexible organic TEGs by reducing the resistance of TE legs and organic−inorganic contacts. Scalable spray printing enables the deposition of micrometer-thick PEDOT:PSS TE legs with a high degree of freedom, resulting in a decreased TE leg resistance, which cannot be achieved by conventional spin coating or drop casting. To reduce the contact resistance, a silane-terminated polystyrene (PS) solution was selectively deposited only onto the contact area, and then highly conductive Ag inks were inkjet-printed to form the interconnects. Chemically coupled PS layers provided additional paths between the PEDOT:PSS and Ag inter-connects that allowed modulation of the primary carrier injection mechanism from thermionic emission to hopping-assisted tunneling.[40,41] Therefore, lower activation energy was required with less temperature dependence for carrier

injection, resulting in a decrease in the contact resistivity. All fabrication processes were performed below plastic-compatible temperatures in an ambient environment.

2. EXPERIMENTAL SECTION

2.1. Fabrication of All-Solution-Processed PEDOT:PSS Thermoelectrics. Figure 1 shows a schematic of the fabrication process, the chemical structure, and a captured image of the all-solution-processed PEDOT:PSS TEGs on a flexible substrate. We prepared glass and polyethylene naphthalate (PEN) substrates and conducted an ultraviolet (UV) ozone treatment to provide sufficiently hydrophilic surface properties for achieving better ink wetting properties. To enhance the conductivity of the PEDOT:PSS TE legs, dimethyl sulfoxide (DMSO, Sigma Aldrich) was added directly into PEDOT:PSS (Clevios PH 1000, Heraeus) with 5 vol % concentration and homogenized with a magnetic stirrer (800 rpm for 3 h at room temperature).[19,42] Then, it was deposited on the prepared substrates using an automatic customized spray printing system (Hantech Co.) with a patterned mask. To deposit highly uniform PEDOT:PSS layers with a film thickness of 1 μm, the printing conditions were carefully optimized with a nozzle height of 14 cm, a printing speed of 30 mm s^{-1}, a pressure of 40 kPa, and a substrate temperature of 80 °C during 12 pass printing. On the patterned PEDOT:PSS TE legs, 0.4 wt % dimethylchlorosilane-terminated PS (PS-Si(CH$_3$)$_2$Cl, M_n = 8 kDa, PDI = 1.06; Polymer Source Inc.) solution dissolved in toluene was treated selectively at the contact region and then annealed on a 100 °C hot plate for 1 h. After rinsing in toluene to remove the uncoupled residues, the nanoparticle-type Ag ink (DGP 40LT-15C, ANP Corp.) was inkjet-printed to form highly conductive interconnects for the series-connected TE legs. The inkjet-printed Ag electrodes were annealed on a 150 °C hot plate for 30 min. All additive fabrication was conducted in an ambient environment. All of the materials were used as received.

2.2. Characterization of PEDOT:PSS Thermoelectrics. To measure the electrical conductivity and Seebeck coefficient, which determine the TE output performance, the PEDOT:PSS TE films with dimensions of 20 mm × 20 mm × 1 μm (width by length by thickness, respectively) were spray-printed on a glass substrate and then annealed at 130 °C for 10 min. The electrical conductivity was calculated using a semiauto sheet resistance/resistivity (R_s/R_{es}) measurement system (Cress Box, Napson Co.), and the film thickness was measured using a stylus-based surface profiler (Alpha-Step IQ, KLA Tencor Co.). The transmittance spectra of PEDOT:PSS films
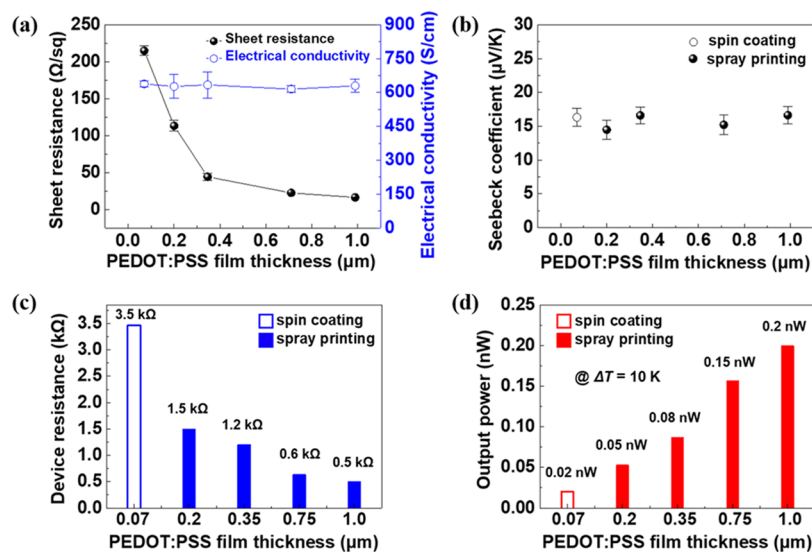
Figure 2. Output performance of 4-leg PEDOT:PSS TEGs with various film thicknesses. (a) Measured sheet resistance and electrical conductivity, (b) Seebeck coefficient, (c) device resistance, and (d) generated output power.
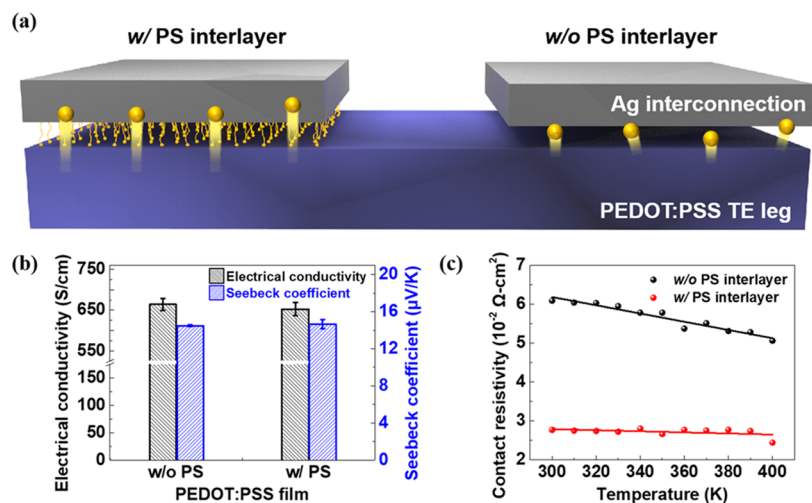
Figure 3. (a) Scheme of carrier injection *via* a PS interlayer between PEDOT:PSS TE legs and Ag interconnects. (b) Measured TE characteristics with and without PS treatment on PEDOT:PSS films. (c) Extracted contact resistivity between the PEDOT:PSS film and the Ag interconnect by the TLM depending on the PS treatment.

were measured in the wavelength range of 300−800 nm using a UV−Vis−NIR spectrometer (V-600, Jasco). The surface roughness of PEDOT:PSS TE layers having different film thicknesses was characterized using a three-dimensional (3D) atomic force microscope (AFM) (XE-100, Park Systems). The Seebeck coefficient was measured using a four-point probe TE measurement system (TEP 600, Seepel Instruments), where the temperature differences of ±0.5, ±1.5, and ±2.5 K were given. To characterize the TE output performance, the fabricated TEGs were placed across two Peltier devices to control the temperature gradients, as shown in Figure S1. Then, the temperature of the hot and cool sides was measured using a thermometer with two thermocouple wires. The measurement of the output performance of the TEGs was carried out when they were in thermal equilibrium.

To extract the surface energy, the contact angle was measured using a contact angle analyzer (Phoenix 10, SEO) at ambient temperature and a relative humidity of 40%. Deionized water (DIW) and ethylene glycol were dropped with a droplet volume of 8 μL onto the PEDOT:PSS films with and without the PS interlayers. The surface energy was calculated from the Owens−Wendt geometric mean equation.[43] The TE output voltage and current were measured using a source meter (Keithley 2400). To determine the surface moieties on the PEDOT:PSS film, X-ray photoelectron spectroscopy (XPS) was conducted with an Al Kα and a power of 6 mA and 12 kV. The contact resistance was analyzed by the transmission line method (TLM) using a semiconductor parameter analyzer (4200-SCS, Keithley) and a probe station system (ST-500, Janis) under vacuum ($\sim$10^{-4} Torr) at various temperatures (from 300 to 400 K).

3. RESULTS AND DISCUSSION

We investigated the TE characteristics of spray-printed PEDOT:PSS layers having different film thicknesses before implementing large-area flexible TEGs. The thickness of the spray-printed PEDOT:PSS films proportionally increased from 200 nm to 1 μm as the number of printing passes increased (Figure S2), whereas the reference spin-coated film had a thickness of 70 nm. It should be noted that the film thickness could increase more than 1 μm *via* spray printing, but the increased adhesion force of the PEDOT:PSS layers with the patterned masks could cause undesirable damage when the masks were detached, as shown in Figure S3. We optimized the conditions for the spray printing process, such as the plate
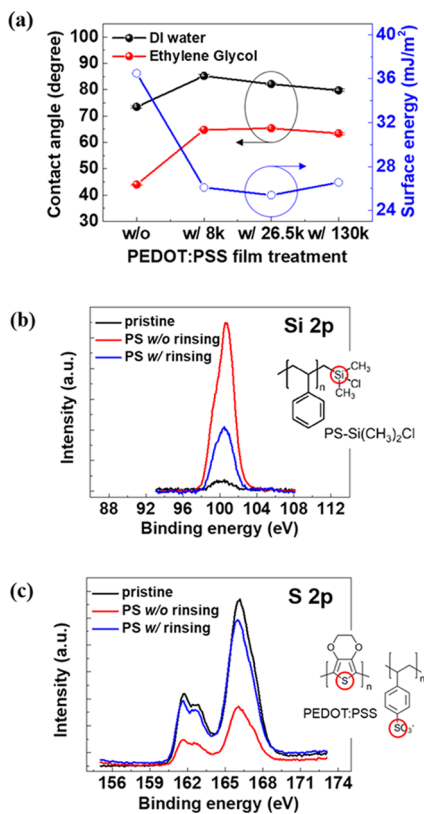
Figure 4. (a) Measured contact angles and extracted surface energies of pristine and PS-treated spray-printed PEDOT:PSS films. XPS spectra for (b) Si 2p and (c) S 2p with and without the PS treatment on PEDOT:PSS films.

temperature, spraying pressure, and nozzle movement speed, which produced uniform PEDOT:PSS layers with a thickness of 1 μm. Upon increasing the number of printing passes, more rough PEDOT:PSS films were produced (Figure S4). Figure 2a,b shows the TE properties of the solution-processed PEDOT:PSS films. The sheet resistance drastically decreased from 215 to 16 Ω sq^{-1} as the film thickness increased from 70

nm to 1 μm, respectively, while their electrical conductivity and Seebeck coefficient of 600 S cm^{-1} and 15 μV K^{-1}, respectively, showed no notable change. These results showed the ability to reduce the resistance of PEDOT:PSS TE legs by optimizing the film thickness without changes in the TE properties *via* additive manufacturing. The electrical resistance, Seebeck coefficient, sheet resistance, surface roughness, and transmittance of the spray-printed PEDOT:PSS films with various thicknesses are summarized in Table S1. Based on the TE properties of these PEDOT:PSS films, planar-type TEGs consisting of 4 legs connected in series by inkjet-printed Ag interconnects were realized. Their resistance was significantly reduced from 3460 to 500 Ω as the film thickness increased from 70 nm to 1 μm (Figure 2c) by employing spray printing, while the other TE properties remained unchanged, indicating that their TE output performance could be enhanced according to eq 1. Figure 2d shows the generated output power of the TEGs with various film thicknesses for ΔT = 10 K. In comparison with the spin-coated PEDOT:PSS TEGs, the open-circuit voltages and the output powers of the spray-printed TEGs were considerably improved from 0.50 to 0.63 mV and from 0.02 to 0.20 nW, respectively. The device resistance and output power of 4-leg PEDOT:PSS TEGs with different film thicknesses are summarized in Table S2. These enhanced output performances were attributed to the reduced internal resistance, especially in the TE leg resistance that resulted from an increase in the film thickness of the TE legs. The overall output voltage and output power were linearly proportional to the increase in ΔT, as shown in Figure S5.

In the perspective of the realization of modules, the contact resistance between the TE layers and interconnects can also significantly affect the module resistance and the corresponding output performance. To improve the contact properties, many strategies for surface treatments have been reported, such as ion implantation to match a work function and organic molecule/polymer binding interlayers for modulating the carrier injection mechanism, especially for field-effect transistors (FETs).[40,41,44] Compatible with low-temperature and large-area additive processing, we introduced an ultrathin end-functionalized PS interlayer between the PEDOT:PSS legs and
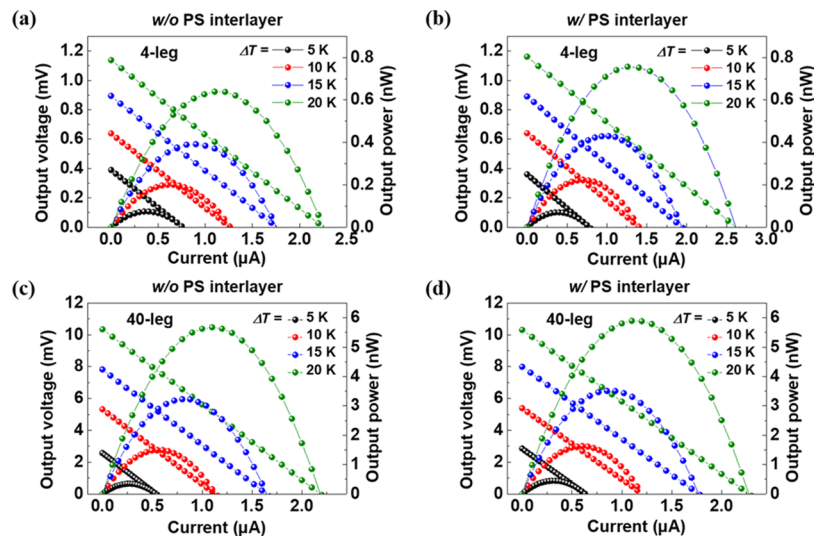
Figure 5. Measured output performances of PEDOT:PSS TEGs with (a, b) 4 legs and (c, d) 40 legs, respectively. After introducing the PS interlayers, the generated output power could be enhanced due to the reduced contact resistance.

Ag interconnects selectively. Note that 4 nm-thick grafted PS layers have been estimated from the results of X-ray spectroscopy in previous reports.[40,41,45,46] A silane-terminated polymer (PS-Si(CH$_3$)$_2$Cl) coupled with a sulfonate group (SO$_3^-$) on a PEDOT:PSS surface provides additional paths for carrier injection. Thus, as shown in Figure 3a, the reduced contact resistance originating from improved charge injection can be expected after introducing a PS interlayer, which is an essential factor for maximizing the output performance of the integrated TEG modules. The electrical conductivity and Seebeck coefficient of the PEDOT:PSS films were not significantly changed after introducing a PS interlayer and had values of ~600 S cm^{-1} and ~15 μV K^{-1}, respectively, which indicates that our interface engineering was compatible with the PEDOT:PSS TE legs (Figure 3b). The contact resistivity between the PEDOT:PSS films and inkjet-printed Ag interconnects was extracted using the TLM. The channel width and thickness of the PEDOT:PSS films were 2 mm and 1 μm, respectively, and the channel length between the electrodes was varied from 1 to 4 mm with a step of 1 mm. Their contact resistance values were determined by extracting the y-intercept from the total resistance versus channel length plots, as shown in Figure S6. The contact resistances of 6.02 × 10^{-2} and 2.77 × 10^{-2} Ω cm^2 were extracted for the interface between the PEDOT:PSS layers and Ag interconnects without and with the PS interlayers, respectively. It should be noted that the contact resistance was significantly reduced when relatively low molecular weight (M_w) (<entanglement M_w of PS, $M_{e,PS}$ = 32 kDa) PS-grafted oxide group (gPS) chains (8 and 26.5 kDa) were introduced, whereas a relatively high-M_w (>$M_{e,PS}$) gPS chain (135 kDa) increased the contact resistance because of lower grafting density.[40] We also calculated the contact resistance of the PEDOT:PSS films with and without PS interlayers at various temperatures from 300 to 400 K, as shown in Figure 3c. In general, the primary carrier injection mechanism at a metal−organic interface is considered to be thermionic emission due to the potential barrier caused by the van der Waals (vdW) gap. The TE device without a PS interlayer exhibited gradually decreasing contact resistance as the temperature increases, which indicates that thermionic emission is the major carrier injection mechanism between the PEDOT:PSS films and inkjet-printed Ag interconnects.[47] On the other hand, the counterpart with a PS interlayer did not show significant temperature dependence of the contact resistance with substantially decreased values, supporting that carrier injection is facilitated through the ultrathin PS interlayer by field emission with an effectively lowered energy barrier. The current−voltage plots of a single TE leg for each temperature also supported these behaviors (Table S3 and Figure S7).

We extracted the activation energy (E_a) using the Richardson equation, as shown in Figures S8 and S9. These results indicate that E_a is lowered after introducing a PS interlayer at the contact region. The difference in the activation energy (ΔE_a) shown in Table S4 was 2.59 ± 0.04 meV on average at a channel length of 1 mm, which is attributed to the change of the primary carrier injection mechanism. These results are consistent with the previous results that field emission can occur if the molecular length is below 4.5 nm, which is a transition point to change the injection mechanism from field emission to hopping.[48] In addition, the resistance for carrier transport by field emission can be expressed as follows

$$R = R_0 \exp(\beta d) \tag{2}$$

where R is the molecular junction resistance, R_0 is the effective contact resistance, β is the tunneling decay coefficient, and d is the molecular length, which indicates that field emission typically exhibits temperature-independent behaviors. The expected thickness of the PS interlayer, ~4 nm, allows that carrier injection is facilitated through the ultrathin PS interlayer by field emission with an effectively lowered energy barrier. To investigate the stability of PS interlayers, we monitored the changes in the contact resistance of PEDOT:PSS TE legs and Ag electrodes with and without a PS interlayer over time (Figure S10). Interestingly, fewer changes in R_c were observed after introducing the PS interlayer exhibiting better environmental stability, which might be attributed to the carrier injection via field emission, not thermionic emission through vdW. In addition, the grafted PS layer could play a role as a passivation layer of PEDOT:PSS TE layers.

The formation of the PS interlayer on the PEDOT:PSS films was clarified via the changed surface energy and XPS spectra. The surface energies of the PEDOT:PSS films with and without PS interlayers were extracted from the Owens−Wendt geometric mean by measuring the contact angles with DIW and ethylene glycol, which are two representative polar and nonpolar solvents, respectively. Figures 4a and S11 show the contact angles and extracted surface energies of the pristine and PS-treated PEDOT:PSS surfaces. The droplets showed the contact angles of approximately 35 and 59° with DIW, and 35 and 55° with ethylene glycol on the pristine and PS-treated PEDOT:PSS film surfaces, respectively. From these results, we found that the surface energy was changed from 36.5 to 26.1 mJ m^{-2} after introducing the PS interlayers. XPS analysis was also conducted to clarify the binding of PS-Si(CH$_3$)$_2$Cl chains with sulfonate (−SO$_3^-$) groups on the PEDOT:PSS film. As shown in Figure 4b, an intense XPS peak at a binding energy of 100.5 eV, corresponding to Si 2p orbitals, is observed when the PS layer was introduced onto the PEDOT:PSS film. This peak was maintained after the toluene rinsing process, while it is difficult to identify the peak for the pristine PEDOT:PSS film. Figure 4c shows another intense peak at a binding energy of 166.1 eV corresponding to S 2p levels of the S atoms in PSS. The strong peak of the pristine PEDOT:PSS film is slightly reduced after forming an ultrathin layer of PS-Si(CH$_3$)$_2$Cl, supporting that silane-terminated PS chains are bound to the −SO$_3^-$ moieties covering the PEDOT:PSS surface. It should be noted that the reduced peak intensity is not attributed to the decrease of PSS as reported in the previous papers.[39,41]

We investigated the effect of interface engineering with PS interlayers on the TE output performance. The output voltages and currents of the planar-type PEDOT:PSS TEGs with 4-leg and 40-leg arranged in series were measured at various ΔT from 5 to 20 K (Figures 5 and S12). Because the total resistances decreased from 506 to 460 Ω and from 4870 to 4542 Ω in average for 4-leg and 40-leg TEGs, respectively, after introducing the PS interlayer, their maximum output powers increased from 200 to 223 pW and from 1.5 to 1.62 nW at ΔT = 10 K, respectively, as shown in Figure 5. These enhanced output performances were attributed to the reduced boundary electrical resistance by modulating the carrier injection mechanism through a PS interlayer. It should be noted that the contact resistance can be changed during the evaluation of TE performance by varying ΔT for the untreated

PEDOT:PSS TEGs. On the other hand, the constant contact resistance was extracted after introducing the PS interlayers due to the changed carrier injection mechanism. Therefore, this approach allows further reliable output power generation regardless of a given temperature difference. Our two strategies, introducing the additive spray printing process and functionalized PS interlayers, could contribute to the enhancement of output performance of about 91 ± 1 and 9 ± 1%, respectively (Tables S5 and S6), and show excellent compatibility to continuous additive manufacturing compared to previous results (Table S7). To demonstrate the processability of large-area and low-temperature printing technologies, all-solution-processed flexible 74-leg PEDOT:PSS TEGs with a PS interlayer were fabricated on a 200 μm-thick PEN substrate. This TEG exhibited an open-circuit voltage of 9.21 mV and an output power of 2.23 nW at ΔT = 10 K, as shown in Figure S13.

4. CONCLUSIONS

We reported two organocompatible strategies to enhance the output performance of all-solution-processed flexible PEDOT:PSS TEGs. The spray printing process enabled us to deposit micrometer-thick PEDOT:PSS TE layers, resulting in much lower internal resistance. The boundary electrical resistance value decreased by more than half by introducing an end-functionalized PS interlayer between the PEDOT:PSS TE layers and Ag interconnects. Thus, continuous printing technologies and interface engineering approaches could reduce the total resistance of TEGs, resulting in an enhanced output performance without changes in other key TE parameters, *i.e.*, the Seebeck coefficient. This work shows a promising approach for the realization of highly integrated flexible organic TEGs using a low-temperature, low-cost, and large-area process.

■ ASSOCIATED CONTENT

Ⓢ Supporting Information

The Supporting Information is available free of charge at https://pubs.acs.org/doi/10.1021/acsami.0c04550.

 PEDOT:PSS thermoelectric leg characterization; thermoelectric performance of all-solution-processed PEDOT:PSS TEGs; contact resistance and activation energy extraction between the spray-printed PEDOT:PSS TE leg and the inkjet-printed Ag electrode; environmental stability of the functionalized polystyrene interlayer (PDF)

■ AUTHOR INFORMATION

Corresponding Authors

Jeonghun Kwak − *Department of Electrical and Computer Engineering, Inter-university Semiconductor Research Center, Seoul National University, Seoul 08826, Republic of Korea;* Ⓞ orcid.org/0000-0002-4037-8687; Email: jkwak@snu.ac.kr

Seungjun Chung − *Photo-Electronic Hybrids Research Center, Korea Institute of Science and Technology, Seoul 02792, Republic of Korea;* Ⓞ orcid.org/0000-0002-4867-4149; Email: seungjun@kist.re.kr

Authors

Seongkwon Hwang − *Photo-Electronic Hybrids Research Center, Korea Institute of Science and Technology, Seoul 02792, Republic of Korea*

Inho Jeong − *Photo-Electronic Hybrids Research Center, Korea Institute of Science and Technology, Seoul 02792, Republic of Korea; School of Electrical Engineering, Korea University, Seoul 02841, Republic of Korea*

Juhyung Park − *Department of Electrical and Computer Engineering, Inter-university Semiconductor Research Center, Seoul National University, Seoul 08826, Republic of Korea*

Jae-Keun Kim − *Department of Physics and Astronomy, and Institute of Applied Physics, Seoul National University, Seoul 08826, Republic of Korea*

Heesuk Kim − *Photo-Electronic Hybrids Research Center, Korea Institute of Science and Technology, Seoul 02792, Republic of Korea*

Takhee Lee − *Department of Physics and Astronomy, and Institute of Applied Physics, Seoul National University, Seoul 08826, Republic of Korea;* Ⓞ orcid.org/0000-0001-5988-5219

Complete contact information is available at:
https://pubs.acs.org/10.1021/acsami.0c04550

Author Contributions

⊥S.H. and I.J. contributed equally to this work.

Notes

The authors declare no competing financial interest.

■ REFERENCES

(1) Bell, L. E. Cooling, Heating, Generating Power, and Recovering Waste Heat with Thermoelectric Systems. *Science* **2008**, *321*, 1457−1461.

(2) Sundarraj, P.; Maity, D.; Roy, S. S.; Taylor, R. A. Recent Advances in Thermoelectric Materials and Solar Thermoelectric Generators-a Critical Review. *RSC Adv.* **2014**, *4*, 46860−46874.

(3) Ren, P.; Liu, Y.; He, J.; Lv, T.; Gao, J.; Xu, G. Recent Advances in Inorganic Material Thermoelectrics. *Inorg. Chem. Front.* **2018**, *5*, 2380−2398.

(4) McGrail, B. T.; Sehirlioglu, A.; Pentzer, E. Polymer Composites for Thermoelectric Applications. *Angew. Chem., Int. Ed.* **2015**, *54*, 1710−1723.

(5) Russ, B.; Glaudell, A.; Urban, J. J.; Chabinyc, M. L.; Segalman, R. A. Organic Thermoelectric Materials for Energy Harvesting and Temperature Control. *Nat. Rev. Mater.* **2016**, *1*, No. 16050.

(6) Martín-González, M.; Caballero-Calero, O.; Díaz-Chao, P. Nanoengineering Thermoelectrics for 21st Century: Energy Harvesting and Other Trends in the Field. *Renewable Sustainable Energy Rev.* **2013**, *24*, 288−305.

(7) Petsagkourakis, I.; Tybrandt, K.; Crispin, X.; Ohkubo, I.; Satoh, N.; Mori, T. Thermoelectric Materials and Applications for Energy Harvesting Power Generation. *Sci. Technol. Adv. Mater.* **2018**, *19*, 836−862.

(8) Zhang, Q.; Sun, Y.; Xu, W.; Zhu, D. Organic Thermoelectric Materials: Emerging Green Energy Materials Converting Heat to Electricity Directly and Efficiently. *Adv. Mater.* **2014**, *26*, 6829−6851.

(9) Hamid Elsheikh, M.; Shnawah, D. A.; Sabri, M. F. M.; Said, S. B. M.; Haji Hassan, M.; Ali Bashir, M. B.; Mohamad, M. A Review on Thermoelectric Renewable Energy: Principle Parameters That Affect Their Performance. *Renewable Sustainable Energy Rev.* **2014**, *30*, 337−355.

(10) Wei, Q.; Mukaida, M.; Kirihara, K.; Naitoh, Y.; Ishida, T. Polymer Thermoelectric Modules Screen-Printed on Paper. *RSC Adv.* **2014**, *4*, 28802−28806.

(11) Wang, L.; Zhang, Z.; Geng, L.; Yuan, T.; Liu, Y.; Guo, J.; Fang, L.; Qiu, J.; Wang, S. Solution-Printable Fullerene/TiS2 Organic/Inorganic Hybrids for High-Performance Flexible n-Type Thermo-electrics. *Energy Environ. Sci.* **2018**, *11*, 1307−1317.

(12) Yan, X.; Poudel, B.; Ma, Y.; Liu, W. S.; Joshi, G.; Wang, H.; Lan, Y.; Wang, D.; Chen, G.; Ren, Z. F. Experimental Studies on Anisotropic Thermoelectric Properties and Structures of N-Type Bi2Te2.7Se0.3. *Nano Lett.* **2010**, *10*, 3373−3378.

(13) Bubnova, O.; Crispin, X. Towards Polymer-Based Organic Thermoelectric Generators. *Energy Environ. Sci.* **2012**, *5*, 9345−9362.

(14) Suh, E. H.; Jeong, Y. J.; Oh, J. G.; Lee, K.; Jung, J.; Kang, Y. S.; Jang, J. Doping of Donor-Acceptor Polymers with Long Side Chains via Solution Mixing for Advancing Thermoelectric Properties. *Nano Energy* **2019**, *58*, 585−595.

(15) Groenendaal, L.; Jonas, F.; Freitag, D.; Pielartzik, H.; Reynolds, J. R. Poly(3,4-Ethylenedioxythiophene) and Its Derivatives: Past, Present, and Future. *Adv. Mater.* **2000**, *12*, 481−494.

(16) Feng-Xing, J.; Jing-Kun, X.; Bao-Tang, L.; Yu, X.; Rong-Jin, H.; Lai-Feng, L. Thermoelectric Performance of Poly(3,4- Ethylenedioxythiophene): Poly(Styrenesulfonate). *Chin. Phys. Lett.* **2008**, *25*, 2202−2205.

(17) Kirchmeyer, S.; Reuter, K. Scientific Importance, Properties and Growing Applications of Poly(3,4-Ethylenedioxythiophene). *J. Mater. Chem.* **2005**, *15*, 2077−2088.

(18) Anno, H.; Nishinaka, T.; Hokazono, M.; Oshima, N.; Toshima, N. Thermoelectric Power-Generation Characteristics of PEDOT:PSS Thin-Film Devices with Different Thicknesses on Polyimide Substrates. *J. Electron. Mater.* **2015**, *44*, 2105−2112.

(19) Ouyang, J.; Xu, Q.; Chu, C. W.; Yang, Y.; Li, G.; Shinar, J. On the Mechanism of Conductivity Enhancement in Poly(3,4-Ethylenedioxythiophene):Poly(Styrene Sulfonate) Film through Solvent Treatment. *Polymer.* **2004**, *45*, 8443−8450.

(20) Li, Z.; Sun, H.; Hsiao, C. L.; Yao, Y.; Xiao, Y.; Shahi, M.; Jin, Y.; Cruce, A.; Liu, X.; Jiang, Y.; Wei, M.; Fei, Q.; Thomas, E.; Simone, F.; Weimin, M. C.; Xinhui, L.; Jens, B.; Joseph, W. B.; Yinhua, Z.; Xavier, C.; Fengling, Z. A Free-Standing High-Output Power Density Thermoelectric Device Based on Structure-Ordered PEDOT:PSS. *Adv. Electron. Mater.* **2018**, *4*, No. 1700496.

(21) Jiang, Q.; Lan, X.; Liu, C.; Shi, H.; Zhu, Z.; Zhao, F.; Xu, J.; Jiang, F. High-Performance Hybrid Organic Thermoelectric SWNTs/PEDOT:PSS Thin-Films for Energy Harvesting. *Mater. Chem. Front.* **2018**, *2*, 679−685.

(22) Besganz, A.; Zöllmer, V.; Kun, R.; Pál, E.; Walder, L.; Busse, M. Inkjet Printing as a Flexible Technology for the Deposition of Thermoelectric Composite Structures. *Procedia Technol.* **2014**, *15*, 99−106.

(23) Wang, X.; Kyaw, A. K. K.; Yin, C.; Wang, F.; Zhu, Q.; Tang, T.; Yee, P. I.; Xu, J. Enhancement of Thermoelectric Performance of PEDOT:PSS Films by Post-Treatment with a Superacid. *RSC Adv.* **2018**, *8*, 18334−18340.

(24) Hossain, S.; Li, T.; Yu, Y.; Yong, J. Recent Advances in Printable Thermoelectric Devices: Materials, Printing Techniques, and Applications. *RSC Adv.* **2020**, *10*, 8421−8434.

(25) Kishi, N.; Kondo, Y.; Kunieda, H.; Hibi, S.; Sawada, Y. Enhancement of Thermoelectric Properties of PEDOT:PSS Thin Films by Addition of Anionic Surfactants. *J. Mater. Sci. Mater. Electron.* **2018**, *29*, 4030−4034.

(26) Zhang, S.; Fan, Z.; Wang, X.; Zhang, Z.; Ouyang, J. Enhancement of the Thermoelectric Properties of PEDOT:PSS: Via One-Step Treatment with Cosolvents or Their Solutions of Organic Salts. *J. Mater. Chem. A* **2018**, *6*, 7080−7087.

(27) Song, H.; Cai, K. Preparation and Properties of PEDOT:PSS/Te Nanorod Composite Films for Flexible Thermoelectric Power Generator. *Energy* **2017**, *125*, 519−525.

(28) Fan, Z.; Li, P.; Du, D.; Ouyang, J. Significantly Enhanced Thermoelectric Properties of PEDOT:PSS Films through Sequential Post-Treatments with Common Acids and Bases. *Adv. Energy Mater.* **2017**, *7*, No. 1602116.

(29) Jin Bae, E.; Hun Kang, Y.; Jang, K.-S.; Yun Cho, S. Enhancement of Thermoelectric Properties of PEDOT:PSS and Tellurium-PEDOT:PSS Hybrid Composites by Simple Chemical Treatment. *Sci. Rep.* **2016**, *6*, No. 18805.

(30) Serrano-Claumarchirant, J. F.; Culebras, M.; Cantarero, A.; Gómez, C. M.; Muñoz-Espí, R. Poly(3,4-Ethylenedioxythiophene) Nanoparticles as Building Blocks for Hybrid Thermoelectric Flexible Films. *Coatings* **2020**, *10*, No. 22.

(31) Bahk, J. H.; Fang, H.; Yazawa, K.; Shakouri, A. Flexible Thermoelectric Materials and Device Optimization for Wearable Energy Harvesting. *J. Mater. Chem. C* **2015**, *3*, 10362−10374.

(32) Wan, C.; Gu, X.; Dang, F.; Itoh, T.; Wang, Y.; Sasaki, H.; Kondo, M.; Koga, K.; Yabuki, K.; Snyder, G. J.; Ronggui, Y.; Kunihito, K. Flexible N-Type Thermoelectric Materials by Organic Intercalation of Layered Transition Metal Dichalcogenide TiS 2. *Nat. Mater.* **2015**, *14*, 622−627.

(33) Testardi, L. R. Calculations of the Thermoelectric Parameters and the Maximum Figure of Merit for Acoustical Scattering. *J. Appl. Phys.* **1961**, *32*, 1978−1981.

(34) Montecucco, A.; Siviter, J.; Knox, A. R. The Effect of Temperature Mismatch on Thermoelectric Generators Electrically Connected in Series and Parallel. *Appl. Energy* **2014**, *123*, 47−54.

(35) Snyder, G. J.; Toberer, E. S. Complex Thermoelectric Materials. *Nat. Mater.* **2008**, *7*, 105−114.

(36) Chung, S.; Jeong, J.; Kim, D.; Park, Y.; Lee, C.; Hong, Y. Contact Resistance of Inkjet-Printed Silver Source-Drain Electrodes in Bottom-Contact OTFTs. *J. Disp. Technol.* **2012**, *8*, 48−53.

(37) Kirihara, K.; Wei, Q.; Mukaida, M.; Ishida, T. Reduction of Specific Contact Resistance between the Conducting Polymer PEDOT:PSS and a Metal Electrode by Addition of a Second Solvent during Film Formation and a Post-Surface Treatment. *Synth. Met.* **2018**, *246*, 289−296.

(38) Taylor, P. J.; Maddux, J. R.; Meissner, G.; Venkatasubramanian, R.; Bulman, G.; Pierce, J.; Gupta, R.; Bierschenk, J.; Caylor, C.; D'Angelo, J.; Zhifeng, R. Controlled Improvement in Specific Contact Resistivity for Thermoelectric Materials by Ion Implantation. *Appl. Phys. Lett.* **2013**, *103*, No. 043902.

(39) Ha, J.; Chung, S.; Pei, M.; Cho, K.; Yang, H.; Hong, Y. One-Step Interface Engineering for All-Inkjet-Printed, All-Organic Components in Transparent, Flexible Transistors and Inverters: Polymer Binding. *ACS Appl. Mater. Interfaces* **2017**, *9*, 8819−8829.

(40) Lee, S.; Jang, M.; Yang, H. Optimized Grafting Density of End-Functionalized Polymers to Polar Dielectric Surfaces for Solution-Processed Organic Field-Effect Transistors. *ACS Appl. Mater. Interfaces* **2014**, *6*, 20444−20451.

(41) Chung, S.; Jang, M.; Ji, S. B.; Im, H.; Seong, N.; Ha, J.; Kwon, S. K.; Kim, Y. H.; Yang, H.; Hong, Y. Flexible High-Performance All-Inkjet-Printed Inverters: Organo-Compatible and Stable Interface Engineering. *Adv. Mater.* **2013**, *25*, 4773−4777.

(42) Kim, J. Y.; Jung, J. H.; Lee, D. E.; Joo, J. Enhancement of Electrical Conductivity of Poly(3, 4-Ethylenedioxythiophene)/Poly-(4-Styrenesulfonate) by a Change of Solvents. *Synth. Met.* **2002**, *126*, 311−316.

(43) Owens, D. K.; Wendt, R. C. Estimation of the Surface Free Energy of Polymers. *J. Appl. Polym. Sci.* **1969**, *13*, 1741−1747.

(44) Cho, K.; Pak, J.; Kim, J. K.; Kang, K.; Kim, T. Y.; Shin, J.; Choi, B. Y.; Chung, S.; Lee, T. Contact-Engineered Electrical Properties of

MoS2 Field-Effect Transistors via Selectively Deposited Thiol-Molecules. *Adv. Mater.* **2018**, *30*, No. 1705540.

(45) Kim, K. J.; Lee, S. M.; Jang, J. S.; Moret, M. Thickness Measurement of a Thin Hetero-Oxide Film with an Interfacial Oxide Layer by X-Ray Photoelectron Spectroscopy. *Appl. Surf. Sci.* **2012**, *258*, 3552−3556.

(46) Martín-Concepción, A. I.; Yubero, F.; Espinós, J. P.; Tougaard, S. Surface Roughness and Island Formation Effects in ARXPS Quantification. *Surf. Interface Anal.* **2004**, *36*, 788−792.

(47) Mahato, S. Composition Analysis of Two Different PEDOT:PSS Commercial Products Used as an Interface Layer in Au/n-Si Schottky Diode. *RSC Adv.* **2017**, *7*, 47125−47131.

(48) Smith, C. E.; Odoh, S. O.; Ghosh, S.; Gagliardi, L.; Cramer, C. J.; Frisbie, C. D. Length-Dependent Nanotransport and Charge Hopping Bottlenecks in Long Thiophene-Containing π-Conjugated Molecular Wires. *J. Am. Chem. Soc.* **2015**, *137*, 15732−15741.